Concentration of Dye-Labeled Nucleotides Incorporated into DNA Determined by Surface Plasmon Resonance-Surface Plasmon Fluorescence Spectroscopy

ARTICLE *in* ANALYTICAL CHEMISTRY · SEPTEMBER 2004

Impact Factor: 5.64 · DOI: 10.1021/ac0495586 · Source: PubMed

3 AUTHORS, INCLUDING:

Sanong Ekgasit
Chulalongkorn University
87 PUBLICATIONS **1,139** CITATIONS

SEE PROFILE

Anal. Chem. **2004,** *76,* 4747−4755

Concentration of Dye-Labeled Nucleotides Incorporated into DNA Determined by Surface Plasmon Resonance-Surface Plasmon Fluorescence Spectroscopy

Sanong Ekgasit,*[,†,‡] Gudrun Stengel,[‡,§] and Wolfgang Knoll[‡]

Sensor Research Unit, Department of Chemistry, Faculty of Science, Chulalongkorn University, Bangkok 10330, Thailand, and Max-Planck-Institut für Polymerforschung, Ackermannweg 10, D-55128 Mainz, Germany

A method for the accurate determination of the fraction of surface-attached DNA duplexes exhibiting a single-fluorophore-labeled nucleobase is introduced. The fluorescence signals obtained from surface plasmon field-enhanced fluorescence spectroscopy along with the optical properties of the sensor architecture determined by surface plasmon resonance were employed for the calculation. A Cy5-labeled nucleotide was incorporated into DNA at a well-defined position via template-directed DNA synthesis performed by a DNA polymerase. The sample-to-sample variations associated with the optical properties of the employed metal films caused a small variation in the strength of the evanescent field. This variation was accounted for by evanescent field integration over the DNA layers. The exponential-type relationship between the fraction of DNA with Cy5-dCTP incorporation at the surface and the mole fraction of the Cy5-dCTP in solution indicates the preferential incorporation of nonlabeled nucleotides by the DNA polymerase.

Surface plasmon resonance (SPR) spectroscopy has been proven to be a powerful affinity biosensor and became an accepted bioanalytical technique for the routine quantification of molecular recognition events at the interfaces.The SPR technique utilizes a surface plasmon wave propagating along the surface of a thin noble metal film to probe the adsorption of thin dielectric films to the metal surface.[1] Hereby, the highly sensitive nature of SPR-based sensors originates from two unique characteristics of the surface plasmon resonance-generated evanescent field at the metal/dielectric interface under total internal reflection conditions. First, the evanescent field is strongly enhanced at the metal/dielectric interface due to resonant coupling between the incident radiation and the surface plasmon wave. Second, this field decays exponentially as a function of the distance from the metal/dielecric interface into the metal film and into the dielectric medium. The accumulation of mass at the metal surface in the course of a reaction causes the interfacial refractive index to change and, hence, changes the resonance angle for surface plasmon excitation. The linear relationship between the SPR signal and the refractive index, thickness change, or both makes SPR a versatile tool for the quantitative analysis of various types of surface interactions.[1,2] While functionalizing a metal surface with thin dielectric films or molecules that undergo specific chemical reactions or molecular recognition events, the physicochemical phenomena at the interface can be selectively followed with high sensitivity.[2] Accordingly, SPR has been extensively employed as an affinity biosensor for monitoring biomolecular interactions at the interface, such as enzyme−substrate, antigen−antibody, receptor−ligand, cell−cell, and drug−protein binding events, and as a highly sensitive technique for monitoring physicochemical phenomena associated with thin films (i.e., chemical reactions, adsorption, degradation, and swelling). A major advantage of SPR is that it offers a label-free and noninvasive method to perform real-time analysis of surface reactions.

In conventional SPR, the resonance angle shift[1c,d] or the reflectance change monitored at a fixed angle of incidence (i.e., an angle slightly lower than the resonance angle)[1b] is employed for observing refractive index, thickness changes, or both of thin, usually nonabsorbing, dielectric films. Although these changes can be detected with high sensitivity, one can further improve the sensitivity of the technique by utilizing the strongly enhanced evanescent field for the excitation of fluorophores. A novel surface-sensitive technique, surface plasmon field-enhanced fluorescence spectroscopy (SPFS), exploits the strong SPR-generated evanescent field for the excitation of a surface-confined chromophore. Monitoring the reflected light and the fluorescence light emitted from the same surface simultaneously enables appreciation of the

* To whom correspondence should be addressed: (e-mail) sanong.e@chula.ac.th.

† Chulalongkorn University.

‡ Max-Planck-Institut für Polymerforschung.

§ Current address: The Scripps Research Institute, 10550 North Torrey Pines Rd., La Jolla, CA 92037.

(1) (a) Raether, H. *Surface Plasmon on Smooth and Rough Surfaces and on Gratings*; Springer-Verlag: Berlin, 1988; Vol. 111. (b) Knoll, W. *Annu. Rev. Phys. Chem.* **1998**, *49*, 569−638. (c) Homola, J.; Yee, S. S.; Gauglitz, G. *Sens. Actuators, B* **1999**, *54*, 3−15. (d) Salamon, Z.; Macleod, H. A.; Tollin, G. *Biochim. Biophys. Acta* **1997**, *1331*, 117−129. (e) Barns, W. L.; Dereux, A.; Ebbesen, T. W. *Nature* **2003**, *424*, 824−830. (f) Liedberg, B.; Lundström, I.; Stenberg, E. *Sens. Actuators, B* **1993**, *11*, 63−72.

(2) (a) Homola, J. *Anal. Bioanal. Chem.* **2003**, *377*, 528−539. (b) Green, R. J.; Frazier, R. A.; Shakesheff, K. M.; Davies, M. C.; Roberts, C. J.; Tendler, J. B. *Biomaterials* **2000**, *21*, 1823−1835. (c) Cooper, M. A. *Anal. Bioanal. Chem.* **2003**, *377*, 834−842. (d) Kasemo, B. *Surf. Sci.* **2002**, *500*, 656−677.

10.1021/ac0495586 CCC: $27.50
Published on Web 07/17/2004

highly sensitive nature of fluorescence spectroscopy in a biosensor format. SPFS has proven to be a complementary technique to SPR spectroscopy since it allows for studies of chemical and physicochemical phenomena occurring at an interface in parallel.[3,4] Moreover, the adsorption of fluorescently labeled low-mass compounds, of a very small number of molecules, or both could be detected in cases where conventional SPR spectroscopy failed.[4,5]

SPR-based biosensors for the specific detection of DNA are widely used as they are sensitive, easy to handle, and do not require the labeling of the target molecules.[2,6] In general, these biosensors require the chemical functionalization of the metal surface with single-stranded (ss) DNA probes that act as catchers for DNA strands with complementary base sequence.[4] If the DNA probes are exposed to the complementary DNA targets, a DNA duplex will be formed. The formation of DNA duplexes at the surface induces refractive index, thickness variations of the functionalized film, or both. If the mass increase during duplex formation is sufficiently large, these changes can be systematically followed using the SPR technique alone. Although the efficiency of the hybridization reaction can be improved by using surface chemistries that optimize the accessibility of the DNA strands, the sensitivity of the fluorescence-based technique is usually superior to that of the SPR-based technique.[3,4] In this work, a technique for the detection of DNA by means of fluorescence without the need for labeling of the target DNA prior to the hybridization reaction is presented. First, the target (template, T) DNA binds to the probe (primer, P) by hybridization of the complementary base sequences. Since this reaction produces a DNA duplex with a recessed 3′ terminus, it can act as a substrate for template-directed DNA synthesis using a DNA polymerase.[8] The enzymatic elongation of the recessed 3′ terminus is initiated by the addition of a mixture of the four different deoxynucleoside triphosphates (dNTPs). In the course of the reaction, the primer strand grows in 5′-to-3′ direction, which finally generates a complete DNA double strand with blunt ends. Here, the incorporation of Cy5-labeled dCTP was employed for labeling of the newly synthesized DNA strand at a specific position opposite to a single guanine base in the template strand. Although the site specificity of the reaction is comparable to that achieved by hybridization of DNA being labeled at the 3′ or 5′ terminus, this reaction has the advantage that the dye is expected to have limited freedom of motion due to its position within the DNA double strand. To eliminate the influence of the distance-dependent fluorescence quenching associated with SPFS fluorescence and to employ the SPFS fluorescence for quantitative analysis, it is essential that the dye molecules are placed at identical distances from the surface in a set of experiments. Moreover, by using this enzymatic reaction, the ultimate number of dye-labeled nucleotides incorporated into the DNA can be easily varied by applying the dye-labeled nucleotides together with unlabeled nucleotides at different mixing ratios.

In general, the SPFS fluorescence signal cannot be employed directly for quantitative analysis due to the distance-dependent fluorescence quenching via the resonance energy transfer to the metal film. The fluorescence intensity is substantially attenuated if the fluorophore is placed too close to the metal film.[9] However, by employing well-defined and reproducible sensor architectures together with physical information from the corresponding SPR curve, the distance-dependent fluorescence quenching can be accounted for. Thus, the quantitative analysis of the SPFS fluorescence signal can be performed. This report will show the quantitative characteristic of the SPFS fluorescence signal derived from the linear relationship between the absorption of light by the fluorophore-containing molecules and the SPR-generated evanescent field at the metal/dielectric interface. The concentrations of DNA double strands containing fluorophore-labeled nucleotides are calculated from the observed SPFS fluorescence. The sample-to-sample variations associated with the complex dielectric constant and the thickness of the metal film are accounted for by correcting the observed SPFS fluorescence with the evanescent field integration over the layer containing fluorophores.

THEORY

Reflectance in the SPR Curve. The SPR reflectance of a multilayer biosensor (i.e., metal film/dielectric films/dielectric substrate) under the Kretschmann−Raether ATR configuration depends strongly on the experimental conditions (i.e., polarization, angle of incidence, and wavelength of the coupled radiation) and on the optical properties (i.e., complex dielectric constant and thickness) of each medium in the sensor architecture. At an angle of incidence greater than the critical angle, the SPR reflectance $R(\theta)$ of the coupled radiation with parallel polarization can be expressed in terms of the evanescent field amplitude and optical

(3) (a) Liebermann, T.; Knoll, W.; Sluka, P.; Herrmann, R. *Colloids Surf., A* **2000**, *169*, 337−350. (b) Liebermann, T.; Knoll, W. *Colloids Surf., A* **2000**, *171*, 115−130. (c) Roy, S.; Kim, J.-H.; Kellis Jr., J. T.; Poulose, A. J.; Robertson, C. R.; Gast, A. P. *Langmuir* **2002**, *18*, 6319−6323. (d) Yu, F.; Yao, D.; Knoll, W. *Anal. Chem.* **2003**, *75*, 2610−2617. (e) Nagamura, T.; Yamamoto, M.; Terasawa, M.; Shiratori, K. *Appl. Phys. Lett.* **2003**, *83*, 803−805.

(4) Neumann, T.; Johansson, M.-L.; Kambhampati, D.; Knoll, W. *Adv. Funct. Mater.* **2002**, *12*, 575−586.

(5) Spinke, J.; Liley, M.; Guder, H.-J.; Angermaier, L.; Knoll, W. *Langmuir* **1993**, *9*, 1821−1825.

(6) Heaton, R. J.; Peterson, A. W.; Georgiadis. R. M. *Proc. Natl. Acad. Sci. U.S.A.* **2001**, *98*, 3701−3704.

(7) (a) Häussling, L.; Schmitt, F.-J.; Knoll, W. *Langmuir* **1991**, *7*, 1837−1840. (b) Jordan, C. E.; Frutos, A. G.; Thiel, A. J.; Corn, R. M. *Anal. Chem.* **1997**, *69*, 4939−4947. (c) Thiel, A. J.; Frutos, A. G.; Jordan, C. E.; Corn, R. M.; Smith, L. M. *Anal. Chem.* **1997**, *69*, 4948−4956. (d) He, L.; Musick, M. D.; Nicewarner, S. R.; Salinas, F. G.; Benkovic, S. J.; Natan, M. J.; Keating, C. D. *J. Am. Chem. Soc.* **2000**, *122*, 9071−9077. (e) Weber, P. C.; Ohlendorf, D. H.; Wendoloski, J. J.; Salemme, F. R. *Science* **1989**, *243*, 85−88. (f) Swalen, J. D.; Allara, D. L.; Andrade, J. D.; Chandross, E. A.; Garoff, S.; Israelachvili, J.; McCarthy, T. J.; Murray, R.; Pease, R. F.; Rabolt, J. F. Wynne, K. J.; Yu, H. *Langmuir* **1987**, *3*, 932−950.

(8) (a) Beese, L. S.; Derbyshire, V.; Steitz, T. A. *Science* **1993**, *260*, 352−355. (b) Kornberg, A.; Baker, T. *DNA Replication*; Freeman: New York, 1992. (c) Krieg, A.; Laib, S.; Ruckstuhl, T.; Seeger, S. *Chem. Biol. Chem.* **2004**, *4*, 589−592. (d) Kuchta, R. D.; Benkovic, P. A.; Benkovic, S. J. *Biochemistry* **1988**, *29*, 6716−6725. (e) Kuchta, R. D.; Mizrahi, V.; Benkovic, P. A.; Johnson, K. A.; Benkovic, S. J. *Biochemistry* **1987**, *26*, 8410−8417. (f) Kunkel, T. A.; Bebenek, K. *Annu. Rev. Biochem.* **2000**, *69*, 497−529.

(9) (a) Barnes, W. L. *J. Mod. Opt.* **1998**, *45*, 661−699. (b) Wokaun, A.; Lutz, H. P.; King, A. P.; Wild, U. P.; Ernst, R. R. *J. Chem. Phys.* **1983**, *79*, 509−514. (c) Lakowicz, J. R. *Anal. Biochem.* **2001**, *298*, 1−24. (d) Pockrand, I.; Brillante, A.; Möbius, D. *Chem. Phys. Lett.* **1980**, *69*, 499−504. (e) Daffertshofer, M.; H. Port, H.; Wolf, H. C. *Chem.* Phys. **1995**, *200*, 225−233.

properties of the materials in the sensor architecture by the following expression.[10]

$$R(\theta) = 1 - A(\theta) = 1 - \left(\frac{2\pi}{\lambda}\right)^2 \frac{1}{k_{zP}(\theta)} \sum_{j=1}^{N} [\int_{z_j}^{z_{j+1}} \mathrm{Im}[\hat{\epsilon}_j]\langle E_z^2(\theta)\rangle \, \mathrm{d}z] \quad (1)$$

where θ is the angle of incidence, $A(\theta)$ is the absorption in *absorptance* units, λ is the wavelength of the coupled radiation, $\hat{\epsilon}_j$ is the complex dielectric constant of the jth layer, and $\langle E_z^2(\theta)\rangle$ is the mean square evanescent electric field at a distance z from the prism/metal interface. N is the number of the dielectric films in the sensor architecture with the metal film as the first layer. $k_{zP}(\theta)$ is the z-component of the wavevector in the prism. $k_{zP}(\theta)$ can be expressed in terms of the x-component of the wavevector $k_{xP}(\theta)$ by $k_{zP}(\theta) = [(2\pi/\lambda)^2\epsilon_P - k_{xP}^2(\theta)]^{1/2}$ with $k_{xP}(\theta) = (2\pi/\lambda)[\epsilon_P \sin^2\theta]^{1/2}$ and ϵ_P is the dielectric constant of the prism. The complex dielectric constant $\hat{\epsilon}$ is related to the complex refractive index by $\hat{\epsilon} = \hat{n}^2 = (n + ik)^2$, where n and k, respectively, are the refractive index and the absorption index. The detailed derivations of the electric field and the SPR reflectance based on the SPR-generated evanescent field are given elsewhere.[10,11]

Absorption by the Dielectric and SPFS Fluorescence Signal. The SPR reflectance of a sensor architecture that contains absorbing dielectric films is governed by the absorption of the metal film and that of the absorbing dielectrics. The reflectance (i.e., with a single layer of an absorbing dielectric) can be expressed in terms of the optical constants of the absorbing components in the sensor architecture and the evanescent field amplitude by[10]

$$R(\theta) = 1 - \left(\frac{2\pi}{\lambda}\right)^2 \frac{1}{k_{zP}(\theta)} \{\int_0^{d_M} \mathrm{Im}[\hat{\epsilon}_M]\langle E_z^2(\theta)\rangle \, \mathrm{d}z + \int_{dAD} \mathrm{Im}[\hat{\epsilon}_{AD}]\langle E_z^2(\theta)\rangle \, \mathrm{d}z\} \quad (2)$$

where d_M and $\hat{\epsilon}_M$, respectively, are the thickness and the complex dielectric constant of the metal film, $\hat{\epsilon}_{AD}$ is the complex dielectric constant of the absorbing layer, and $\int_{dAD}$ indicates an integration over the absorbing dielectric film.

In conventional SPR spectroscopy, the absorption of the dielectric film cannot be measured separately from that of the metal film. However, by fabricating the sensor surface stepwise and fitting the observed SPR curves with the Fresnel equation, the optical properties of each layer of the sensor surface can be obtained. Thus, absorption of each layer can then be calculated (i.e., via eq 1). If the absorbing dielectric film contains fluorophores, the absorption of the dielectric film can be observed independently from the fluorescence emission using the SPFS technique. Although there is a linear relationship between the fluorescence intensity and the absorption by fluorophores, the SPFS fluorescence is attenuated by the fluorescence quenching via nonradiative resonance energy transfer (RET) to the metal film. Due to the distance-dependent nature of the RET phenomenon, the SPFS fluorescence exhibits strong distance-dependent behavior.[3b,4] The SPFS fluorescence decreases substantially if the fluorophores are confined too close to the metal film. The angle-dependent SPFS fluorescence can be expressed in terms of the evanescent field amplitude and the optical properties of the fluorophore-containing dielectric film by[10]

$$i_{\mathrm{fluorescence}}(\theta) = K_{\mathrm{optics}}\left(\frac{2\pi}{\lambda}\right)^2 \frac{1}{k_{zP}(\theta)} \int_{\mathrm{dfluorophore}} K_{\mathrm{RET}}(z) \, \mathrm{Im}\,[\hat{\epsilon}_{\mathrm{fluorophore}}]\langle E_z^2(\theta)\rangle \, \mathrm{d}z \quad (3)$$

where $\int_{\mathrm{dfluorophore}}$ indicates an integration over the thickness and the complex dielectric constant of the fluorophore-containing dielectric film. $K_{\mathrm{RET}}(z)$ is the distance-dependent RET fluorescence quenching factor. K_{optics} is a constant. It should be noted that K_{optics} depends strongly on the experimental parameters (i.e., laser intensity, optical filter, focusing lens, and optical windows).

Although the parameters associated with the nonabsorbing components of the sensor architecture do not appear in the equations above, they influence the observed SPR and SPFS curves. The resonance angle and the fluorescence angle (i.e., the angle with the maximum fluorescence) shift to greater values as the thickness, refractive index, or both of the nonabsorbing dielectric increase. The nonabsorbing dielectric film (i.e., located between the metal film and the fluorophore-containing dielectric film) serves as a spacer that increases the distance between the fluorophore and the metal surface in order to reduce the quenching of the emitted fluorescence.[3b,4] Since the evanescent field amplitude has an exponential decay characteristic, its strength is already weakened when the field penetrates the absorbing layer on top of the nonabsorbing film. By keeping the distance between the fluorophore-containing film and the metal surface constant for a set of experiments through the use of well-defined, controllable surface chemistries (i.e., via self-assembled monolayers and specific binding reactions),[7] comparable quenching efficiencies can be achieved. However, to employ the observed SPFS fluorescence for the quantitative analysis of a particular system, the sample-to-sample variation associated with the optical properties of the metal film must be corrected by evanescent field integration over the fluorophore-containing layer. The evanescent field can be calculated from the fitting parameters of the corresponding SPR curve.[10]

EXPERIMENTAL SECTION

SPR-SPFS Setup. For SPR measurements, the radiation of a HeNe laser (λ = 632.8 nm, 5 mW, Uniphase) was modulated by a chopper. The plane of polarization and the intensity of the modulated radiation were controlled by two Glan-Thompson polarizers. The radiation was coupled to the sensor architecture via a rectangular prism (LaSFN9, ϵ = 3.4036, Helma Optik) in the Kretschmann configuration. The reflected beam was focused toward a photodiode detector using a lens (f = 50 mm, Owis). In parallel to the reflectance measurement, the corresponding SPFS fluorescence signal was collected from the backside of the prism. The fluorescence light was focused using a lens (f = 50 mm, Owis), passed through a neutral filter and an interference filter (λ = 670 nm, $\Delta\lambda$ = 10 nm, LOT, 80% transmission), before being measured by a photomultiplier tube (PMT, Hamamatsu). The PMT was connected to a photon counter unit (Agilent) where the

(10) (a) Ekgasit, S.; Thammacharoen, C.; Yu, F.; Knoll, W. *Anal. Chem.* **2004**, *76*, 561−568. (b) Ekgasit, S.; Thammacharoen, C.; Yu, F.; Knoll, W. *Anal. Chem.* **2004**, *76*, 2210−2219.

(11) Hansen, W. N. *J. Opt. Soc. Am.* **1968**, *58*, 380−390.

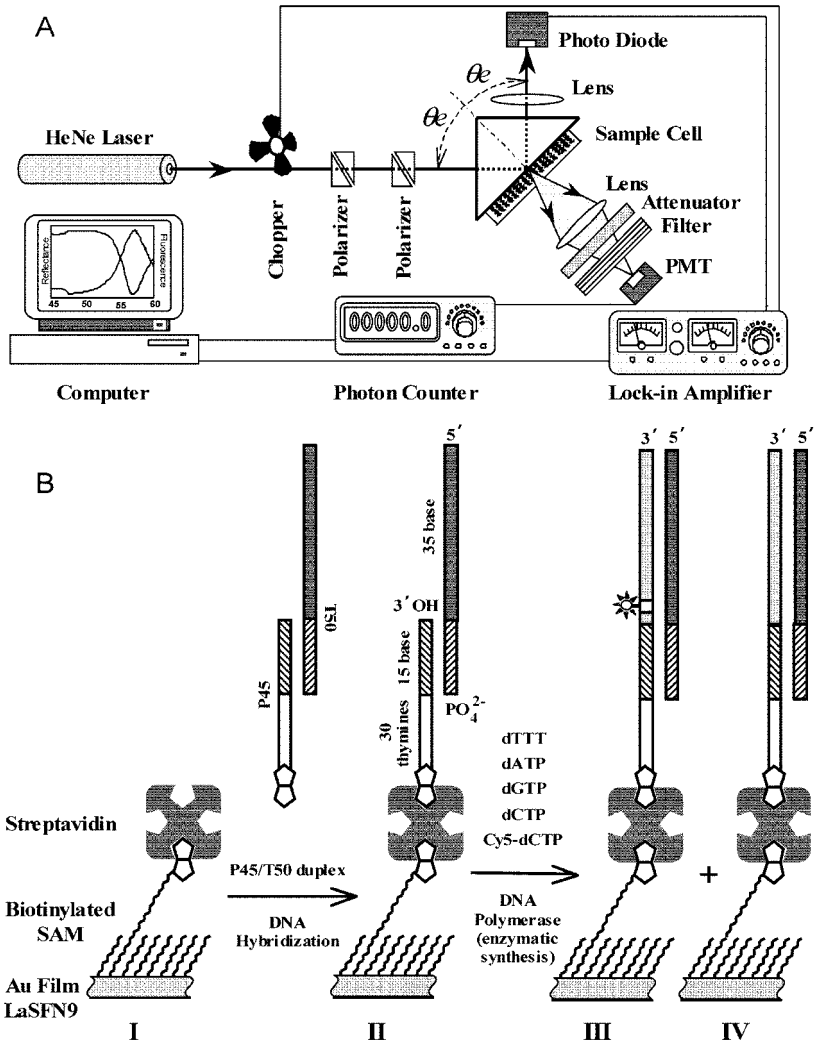

Figure 1. (A) Schematic illustration of the employed SPR-SPFS experimental setup. (B) Schematic drawings of the biosensor architecture: (I) streptavidin-functionalized SAM; (II) immobilized P45/T50 duplex on sensor surface; (III) complete double-strand P45/T50with Cy5-dCTP incorporation; and (IV) complete double-strand P45/T50. The position of the guanine base on the template strand T50, where the Cy5-dCTP incorporation takes place, is shown.

fluorescence signal was acquired as photon counts per second. The neutral filter attenuated the fluorescence signal to be within the photomultiplier's linear range (i.e., less than 1.5×10^6 counts/s). The current experiments utilized a 1.3 dB attenuation (i.e., the fluorescence intensity was attenuated by 20 times). A schematic illustration of an SPR-SPFS setup is shown in Figure 1.

The SPR-SPFS signals were collected as a function of the measure incidence angle θe defined relative to the surface normal of the prism/metal interface. Due to the refraction at the air/prism interface, the measured incidence angle θe is slightly different from the actual angle of incidence θ at the prism/metal interface. The relationship between the two angles is given by $\theta e = \sin^{-1}[\epsilon_P^{1/2} \sin(\theta - \varphi)] + \varphi$, where $\varphi = 45°$ for a rectangular prism.

Preparation of the Sensor Chip. LaSFN9 glass wafers (20 × 20 × 2.5 mm, $\epsilon = 3.4036$, Helma Optik) were cleaned and coated with a ~1-nm chromium film in order to improve the adhesion and stability of the gold film. The chromium-coated glass wafers where then coated with a ~45-nm gold film via a commercially available thermal evaporation instrument (Edwards FL400) at a deposition rate of 0.1 nm/s under the ultrahigh vacuum condition. The self-assembled monolayer (SAM) of biotinylated thiols was prepared ex situ by immersing the gold-coated LaSFN9 wafers in a binary mixture of thiols in absolute ethanol overnight at room temperature. The binary mixture contained a long-chain biotin-terminated thiol (11-mercapto(8-biotinamido-4,7-dioxaoctyl)undecanoylamide, 0.5×10^{-4} M) and a short-chain OH-terminated thiol (11-mercaptoundecanole, 4.5×10^{-4} M) acting as a lateral spacer. During the incubation, the sensor wafer was kept in the ethanol-saturated atmosphere. The substrates were rinsed thoroughly with absolute ethanol and blown-dry with dry nitrogen before they were mounted onto the flow cell for SPR-SPFS measurements. The flow cell was connected to a peristaltic pump (Ismatec) and the sample reservoir using Tygon tubes with an inner diameter of 0.76 mm. Thus, a closed circulation loop was formed, which was disconnected during the injection phase. The total volume of the loop amounted to 300 μL; therefore, injection volumes between 1 and 1.5 mL have been used to ensure the desired analyte working

concentration. All measurements were performed upon a constant flow rate of 2 mL/min. Routinely, a SPR experiment started with recording the changes of reflectivity as a function of the incidence angle (angle scan) for the thiol-coated gold surface immersed in PBS buffer (10 mM phosphate buffer, 2.7 mM KCl, 150 mM NaCl, pH 7.4). Thereafter, the surface modification step was followed in the kinetic mode of the instrument by choosing a fixed angle of incidence and monitoring the reflectivity as a function of time. By definition, the angle chosen for kinetic measurements was the one corresponding to 30% reflectivity, which ensured that the reflectivity changed linearly with the resonance angle. After a new equilibrium was reached, the surface was rinsed with PBS buffer and a second scan spectrum was monitored.

In a first step, the streptavidin (Roche) was bound onto the biotinylated SAM from a 1 μM solution in physiological PBS buffer. In a second step, the DNA film was prepared by exposure of the P45/T50 duplex to the streptavidin layer (1 μM in PBS). The P45/T50 duplex was prepared ex situ by annealing of the primer oligonucleotide P45 (5′-biotin-$(T)_{30}$-ACG TCA GTC TCA CCC-3′, MWG Biotech) with the template strand T50 (5′-AGT TAC AGA GGT AGT AGT GGC TGA GTG AAT ATT **G**T G GGT GAG ACTGAC GT-3′, MWG Biotech) in PBS buffer for 1 h (final duplex concentration 50 μM). The complementary parts of the oligonucleotide sequences are underlined, and the single guanine base that will be paired with Cy5-dCTP in the course of the polymerization process is shown as a boldface character. The hybridization reaction created a DNA duplex that exhibited a 5′overhang of 35 bases acting as a template for the synthesis of the complete double strand. All previously described reaction steps as well as the following polymerase reactions were carried out at 22 °C.

Polymerase Reactions. After it had been confirmed by SPR scan spectra that the various surfaces exhibited equal amounts of DNA duplexes, the primer extension assays were carried out employing the exonuclease-free mutant of the Klenow fragment (purchased from Amersham Pharmacia Biotech). For this purpose, we switched from PBS to HSM buffer (10 mM HEPES, pH 7.4, 150 mM NaCl, 10 mM $MgSO_4$) to provide the necessary Mg^{2+} ions as a cofactor. Using the kinetic mode, the adsorption of the Klenow fragment (8 nM) was followed until the binding reaction reached its equilibrium. Than, a mixture of all four unlabeled dNTPs and Cy5-dCTP (purchased from Amersham Pharmacia Biotech) at a fixed total concentration of 1 μM each was added to initiate the polymerization reaction. When a constant fluorescence intensity indicated the end of the polymerization process, unincorporated dye was removed by rinsing with HSM buffer. Before monitoring the SPFS scan spectra, we switched back to PBS buffer in order to ensure identical bulk refractive indexes and to disable further polymerization by removal of the cofactor. The enzymatic reaction was performed at various mole fractions of Cy5-dCTP (i.e., $\chi = 1.00$, 0.90, 0.75, 0.50, 0.25, and 0.00) using different gold-coated glass wafers. Note: The template strand T50 contained only one guanine base; thus, a single Cy5-dCTP was incorporated per DNA substrate at an identical position. The schematic illustration of the functionalization of the biotinylated SAM with streptavidin molecules, the DNA immobilization, and the subsequent enzymatic elongation of the DNA strands are shown in Figure 1.

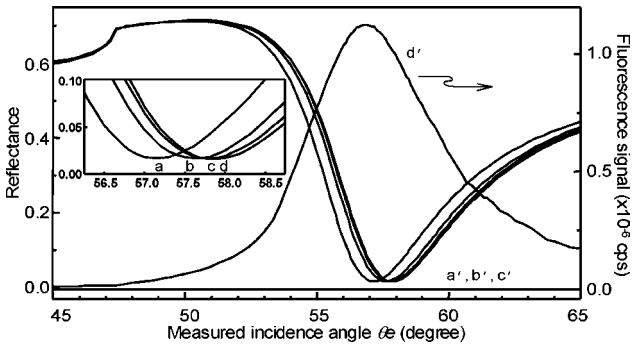

Figure 2. SPR-SPFS curves of the biosensor under the enzymatic synthesis with mole fraction of Cy5-dCTP $\chi = 1$: (a) biotinylated SAM, (b) SAM/streptavidin, (c) SAM/streptavidin/(P45/T50) duplex, and (d) SAM/streptavidin/ds-(P45/T50) with Cy5-dCTP incorporation. The corresponding SPFS curves are represented by a′, b′, c′, and d′.

RESULTS

Figure 2 shows SPR scan curves for the stepwise functionalization of the thiol-coated gold surface with streptavidin and biotinylated DNA and the result of its enzymatic extension carried out at a mole fraction of Cy5-dCTP $\chi = 1.00$. Each adsorption process was observed in the kinetic mode (data not shown), and nonadsorbed bulk material was removed by rinsing with PBS buffer prior to monitoring the SPR scan curves. As the thickness of the dielectric film increases, the resonance angle shifts to a greater value without a significant change in the depth of the reflectance minimum. The largest increment was observed when streptavidin was bound onto the biotinylated thiol SAM (Figure 2b). A smaller resonance angle shift was observed when the prehybridized duplex P45/T50 was bound to streptavidin layer (Figure 2c). Curves d and d′ correspond to the simultaneously recorded reflectivity and fluorescence changes, respectively, which resulted from the enzymatic elongation of the immobilized duplex P45/T50. This reaction produced a complete DNA double strand that carried a Cy5-labeled cytidine base at a single defined position of the sequence. Although only a very small resonance angle shift was observed when the duplex P45/T50 underwent enzymatic synthesis accompanied by the incorporation of Cy5-dCTP (Figure 2d), a strong fluorescence signal from the corresponding SPFS curve was observed. The exposure of the dNTP mixture to the DNA film in the absence of the DNA polymerase did cause a small background fluorescence (due to bulk molecules excited in the evanescent field of the surface plasmon) that could be quantitatively removed by buffer rinsing within seconds. Since the scan spectra were always recorded after the rinsing step, unspecific adsorption can be ruled out as a reason for the fluorescence increase. There was no detectable change of the fluorescence signal in the angle scan SPFS curves prior to the enzymatic reaction (Figure 2a′, b′, and c′).

Similar changes such as displayed in Figure 2 were observed in the SPR-SPFS experiments where the extension reaction was performed using lower mole fractions of Cy5-dCTP in the mixed dNTPs solution. While the resonance angles also remained unchanged for lower mole fractions χ, the SPFS fluorescence decreased as the mole fraction of Cy5-dCTP decreased (SPR-SPFS curves are available in the Supporting Information).

Figure 3 shows SPR-SPFS curves of the completed double-strand P45/T50 after enzymatic extension at different mole fraction

Table 1. Fitting Parameters, Resonance Conditions, and Fluorescence Conditions of the SPR-SPFS Curves in Figure 3

	optical properties of the sensor architecture[a] complex dielectric constant ($\hat{\epsilon} = \epsilon' + i\epsilon''$) **thickness** (nm)						SPR[b] θ_{SPR}	SPFS[b] $\theta_{fluorescence}$
χ	Cr[c]	Au	SAM	SA[d]	DNA[e]	DNA[f]	***R***	**I** ($\times 10^{-6}$ counts/s)
1.00	$-5.62 + i31.95$	$-12.88 + i1.46$	2.25	2.1025	1.8903	1.8903	57.9°	56.9°
	0.6	**40.3**	**1.5**	**3.4**	**3.5**	**1.4**	**0.016**	**1.124**
0.90	$-5.62 + i31.95$	$-12.90 + i1.43$	2.25	2.1025	1.8903	1.8903	57.7°	56.9°
	0.5	**40.5**	**1.5**	**3.4**	**3.4**	**1.4**	**0.018**	**0.602**
0.75	$-5.62 + i31.95$	$-12.80 + i1.42$	2.25	2.1025	1.8903	1.8903	57.9°	57.1°
	0.6	**40.9**	**1.5**	**3.5**	**3.4**	**1.4**	**0.015**	**0.277**
0.50	$-5.62 + i31.95$	$-12.67 + i1.49$	2.25	2.1025	1.8903	1.8903	57.8°	57.2°
	0.5	**46.6**	**1.5**	**3.4**	**3.4**	**1.9**	**0.006**	**0.167**
0.25	$-5.62 + i31.95$	$-12.78 + i1.58$	2.25	2.1025	1.8903	1.8903	57.7°	57.1°
	0.5	**45.5**	**1.6**	**3.6**	**3.4**	**1.0**	**0.005**	**0.101**
0.00	$-5.62 + i31.95$	$-12.78 + i1.58$	2.25	2.1025	1.8903	1.8903	57.9°	n/a[g]
	0.5	**40.3**	**1.5**	**3.5**	**3.4**	**1.4**	**0.017**	**n/a**

[a] An LaSFN9 glass ($\hat{\epsilon} = 3.4036$) is employed as a right-angled coupling prism while the PBS buffer ($\hat{\epsilon} = 1.778$) is employed as a semi-infinitely thick nonabsorbing dielectric substrate. [b] The measured incidence angle θe has a resolution of 0.2° near the resonance angle. [c] From ref 13c. [d] Streptavidin. [e] Layer of immobilized duplex P45/T50 (before the enzymatic reaction). [f] Layer of complete double-strand P45/T50 with Cy5-dCTP incorporation (after the enzymatic reaction). [g] The observed fluorescence signal is within the noise level; thus, $\theta_{fluorescence}$ cannot be defined.

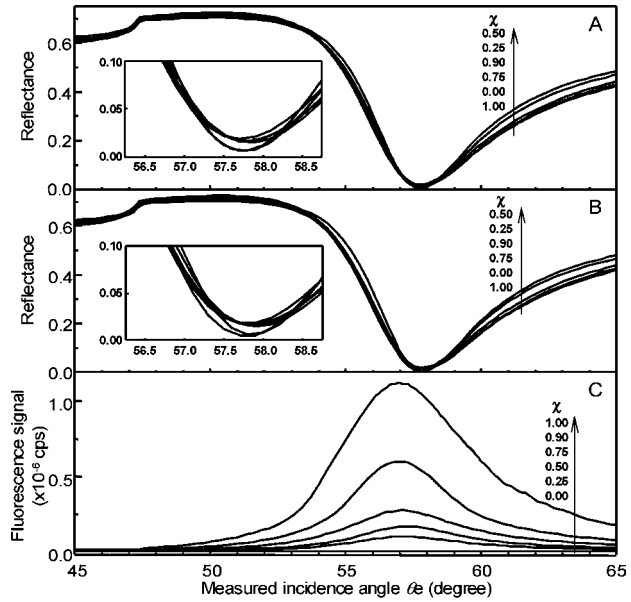

Figure 3. (A) SPR curves of the immobilized P45/T50 duplex prior to the enzymatic synthesis, (B) SPR curves, and (C) the corresponding SPFS curves of the complete double-strand P45/T50 after the enzymatic synthesis at various mole fraction χ of Cy5-dCTP in the mixed dNTPs solution. The inset shows resonance condition of the SPR curves. Since the sensor architectures are carefully fabricated, the SPR curves show small variations associated with the optical constants of the metal film. The associated sensor architectures, resonance, and fluorescence conditions are shown in Table 1.

χ. For a better comparison, the SPR scan curves monitored prior to performing the primer extension reaction are shown in Figure 3A (the corresponding SPFS curves are not shown since no chromophore had been involved yet; see Figure 2c′). The SPR and SPFS curves of the completed DNA duplexes are shown in Figure 3B and C, respectively. While only minor differences were observed among the SPR curves in Figure 3B, the corresponding SPFS curves in Figure 3C showed strong concentration-dependent characteristics. Here, the fluorescence intensity was substantially decreased as the mole fraction χ decreased. However, a linear relationship between the mole fraction χ and the fluorescence intensity at the florescence angle was not observed. According to Figure 3B and C, the fluorescence angle of the SPFS curve is always slightly lower than the resonance angle of the corresponding SPR curve. The observed resonance angles and the observed fluorescence angle are summarized in Table 1. The optical properties of the metal and the dielectric films were obtained from fitting the observed SPR curves with the Fresnel equation and are shown in Table 1. A comparison between the observed SPR curves and the corresponding theoretically calculated curves is available in the Supporting Information. It should be noted that the double-strand P45/T50 with Cy5-dCTP incorporation has a nonzero imaginary part of the complex dielectric constant. In these experiments, the imaginary part of the complex dielectric constant is very small. Thus, the absorption is too small to induce any significant changes in the minimum reflectance of the SPR curve although the maximum possible mole fraction χ of the Cy5-dCTP was employed; see Figure 2. However, the nonzero imaginary part of the complex dielectric constant can be observed by the strong SPFS fluorescence signal associated with the SPR excitation. Since the concentration of the fluorescence dye in the double-strand P45/T50 layer is very low, no self-quenching by neighboring dye molecules is assumed in the further calculations.

DISCUSSION

As expected, the resonance angle and the fluorescence angle shift to greater angles with increasing thickness or refractive index of the dielectric film. The fluorescence signal is due to the excitation of chemically bound Cy5 fluorophores via the strong SPR-generated evanescent field. Although the reflection loss in SPR curves and the fluorescence emission in the SPFS curves are governed by the same SPR-generated evanescent field, there is a discrepancy between the resonance angle and the angle of the maximum fluorescence emission. This can be reasoned by the wave vector-dependent natures and the decay characteristics of the evanescent field in the metal film and in the dielectric media. These unique characteristics make the fluorescence angle always slightly smaller than that of the corresponding resonance angle.[10b]

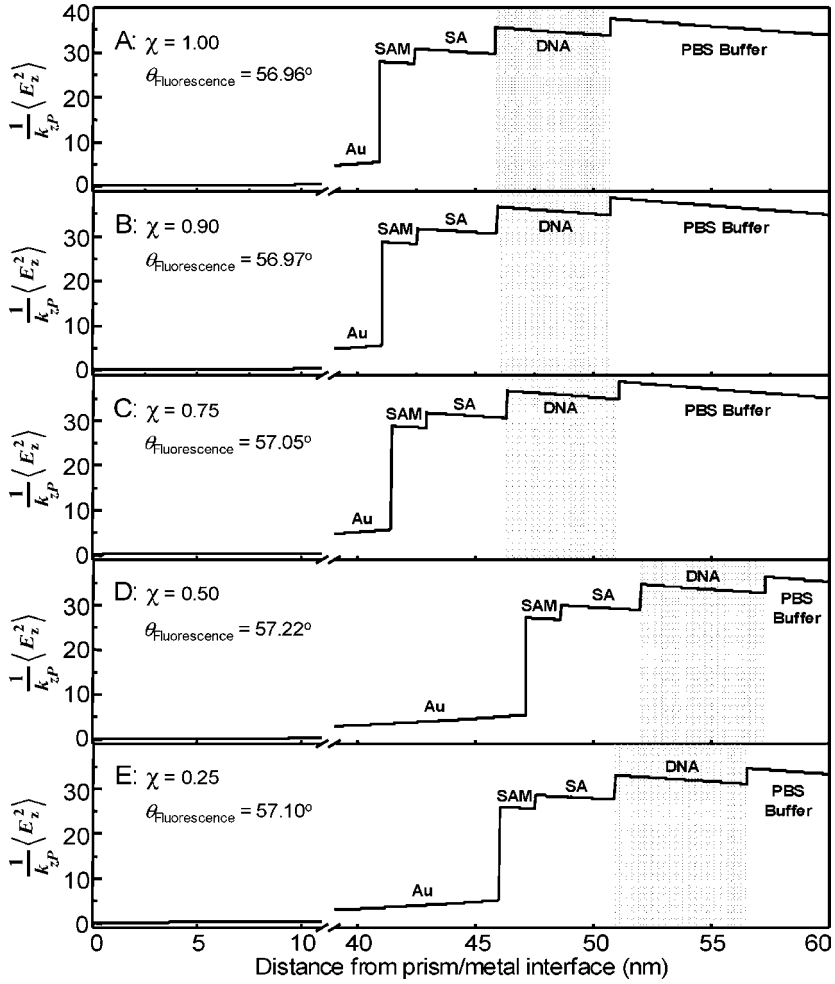

Figure 4. MSEF decay profiles at the fluorescence angles of SPFS curves in Figure 3C. The shaded areas indicate the complete double-strand P45/T50. The step increments indicate interfaces between two consecutive layers in the sensor architecture with different dielectric constants. Note: the fluorescence angles are obtained from the theoretical calculation based on the sensor architectures in Table 1.

Since the presented DNA films were nonabsorbing or weakly absorbing, only an insignificant change in the depth of the reflectance minimum was observed as the resonance angle shifted to greater values. When the immobilized duplex P45/T50 was subjected to the enzymatic reaction and Cy5-dCTP was incorporated into the growing DNA strand, a very small resonance angle shift was observed due to a small increase of the thickness of the DNA layer (see the corresponding SPR curves in Figure 3A and B). The strong fluorescence signal of the corresponding SPFS curves in Figure 3C indicates the superior sensitivity of the SPFS technique compared to that of SPR spectroscopy. Although a 1.3 dB attenuator was employed, a strong fluorescence signal was still observed. The SPFS curves also showed a strong concentration dependence of the fluorescence signals. The small discrepancies of the resonance angles of the SPR curves depicted in Figure 3B (and within Figure 3A) indicate similar optical properties and associated changes of the dielectric film due to physicochemical phenomena at the sensor surface as the mole fraction χ increases. The SPR curves of the biotinylated SAMs prior to the functionalization with streptavidin are available in the Supporting Information. Due to the well-defined and reproducible nature of the sensor architecture, similar SPR curves were observed throughout the experiments. The small discrepancy of the SPR curves shown in Figure 3A and B are attributed to the sample-to-sample variation of the optical property of the employed metal films.

Due to the well-defined structures and the reproducibility of the employed sensor architectures, as shown in Table 1, the fluorophores were subjected to evanescent fields of similar strength, and hence, they were quenched to the same extent. This is the prerequisite for the quantitative analysis of the observed SPFS fluorescence signals. However, the sensor-to-sensor variation associated with the optical properties of the metal films makes the SPR-generated evanescent field at each sensor surface slightly different. As a result, fluorophores in different samples are subjected to different evanescent field amplitudes. Although the imaginary part of the dielectric constant is very small and cannot be differentiated from that of the nonabsorbing dielectric via the SPR technique (i.e., via the shift of the reflectance minimum), the fraction of the complete double-strand P45/T50 with C5-dCTP incorporation can be calculated from the highly sensitive SPFS fluorescence. According to eq 3, the fluorescence intensity is proportional to the integration of the product between the imaginary part of the dielectric constant of the absorbing dielectric and the evanescent field amplitude. To calculate the fraction of the complete double-strand P45/T50 with Cy5-dCTP incorporation

Table 2. Fraction of the Complete Double-Strand P45/T50 with Cy5-dCTP Incorporation $\chi_{surface}$ at Various Mole Fractions χ of Cy5-dCTP in the Mixed dNTPs Solution

χ	fluorescence signal at $\theta_{fluorescence}$ ($\times 10^{-6}$ counts/s)	evanescent field integration[a]	incorporation fraction $\chi_{surface}$
1.00	1.124	1.475	1.00
0.90	0.602	1.488	0.54
0.75	0.277	1.487	0.25
0.50	0.167	1.541	0.16
0.25	0.101	1.558	0.09
0.00[b]	n/a (noise level)	n/a	0.00

[a] The evanescent field integration (at $\theta_{fluorescence}$) over the thickness of the complete double-strand P45/T50 after the enzymatic synthesis (i.e., the shaded area in Figure 4 with DNA labeled). [b] The observed fluorescence signal is within the noise level; thus, $\theta_{fluorescence}$ cannot be defined and the evanescent field integration cannot be calculated.

precisely, the differences in the evanescent field amplitudes associated with the optical constant of the metal film have to be accounted for. Based on the data for the sensor architecture in Table 1, the mean square evanescent field profiles within the sensor architecture at the fluorescence angles have been calculated and are shown in Figure 4. The corresponding evanescent field integrations over the DNA layer are shown in Table 2.

Although K_{optics} and K_{RET} are not known, they are constant and have the same value for all measurements due to the same experimental setup and the well-defined sensor architecture. If 100% efficiency of the Cy5-dCTP incorporation is assumed at a mole fraction of Cy5-dCTP $\chi = 1.00$, the relative fraction of the complete double-strand P45/T50 with Cy5-dCTP incorporation, $\chi_{surface,}$ at any other mole fraction χ can be calculated from the SPFS fluorescence at the fluorescence angle, according to eq 3, by

$$\chi_{surface} = \frac{\left\{I_{fluorescence}(\theta_{fluorescence})/\left[\frac{1}{k_{zP}(\theta_{fluorescence})}\int_{dfluorophore}\langle E_z^2(\theta_{fluorescence})\rangle\,dz\right]\right\}\Big|_{\chi}}{\left\{I_{fluorescence}(\theta_{fluorescence})/\left[\frac{1}{k_{zP}(\theta_{fluorescence})}\int_{dfluorophore}\langle E_z^2(\theta_{fluorescence})\rangle\,dz\right]\right\}\Big|_{\chi=1}} \quad (4)$$

Figure 5 shows a plot of the relative fraction $\chi_{surface}$ versus the mole fraction χ of Cy5-dCTP in the mixed dNTPs solution. The fraction of the complete double-strand P45/T50 with incorporated Cy5-dCTP decreased substantially as the concentration of the nonlabeled dCTP increased. The exponential-type relationship implies that the enzymatic reaction does not follow a statistical mechanism, rather, the DNA polymerase prefers the incorporation of the nonlabeled dCTP. This finding is in good agreement with previous results addressing the label efficiency in dependence of the chemical nature of the attached dye, the linker moiety used for attachment of to the dNTP and the nucleobase to which the dye was attached.[14] Utilizing PCR, random priming or nick translation as labeling techniques, these studies agreed in that it was hardly possible to achieve quantitative substitution of a

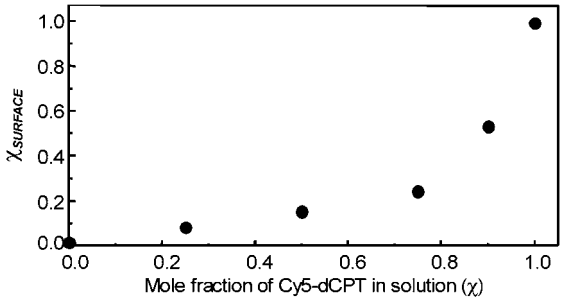

Figure 5. Fraction of the complete double-strand P45/T50with Cy5-dCTP incorporation on the biosensor surface $\chi_{surface}$ at various mole fractions χ of Cy5-dCTP in the mixed dNTPs solution.

nucleotide by its labeled analogue in long DNA fragments requiring frequent additions of the respective nucleotide. Instead, an inverse relationship was found between modified DNA product yield and the content of incorporated dye-dNTPs. Thus, the number of chain termination events increased with an increasing number of dye labels present in the primer strand. Although, the exact nature of the interaction between the DNA polymerase and the growing DNA chains is not fully understood, a number of reasons have been proposed to explain the variation between natural and modified substrates: among them is the altered geometry of the dNTP, changes in the solubility of the dNTP, steric hindrance due to bulkiness of the molecule, and hydrophobic interactions between the enzyme and the incorporated dye leading to stalling or dissociation of the polymerase. Zhu and Waggoner[14b] confirmed that the impairment of the polymerase function is reduced with increasing length of the linker moiety. Moreover, they found that modifications of the template strand are less inhibitive than those of the primer strand but they interfere with primer hybridization in PCR reactions, which also provokes reduced yields. The design of our experiments is different in that it examined incorporation of dNTPs at a single site of the DNA strand. Consequently, processes that are relevant in PCR reactions, such as primer hybridization after duplex melting or rebinding of the enzyme to heavily labeled DNA regions, did not play any role. Hence, our result demonstrates that discrimination between labeled and unlabeled dNTP substrates occurs during the early stage of nucleotide selection and the reduced labeling yield is not entirely a consequence of perturbed interactions between the DNA polymerase and the already labeled primer/template duplex.

In the present work, SPFS was shown to be a very sensitive method for the detection of DNA achieved by the extension of the primer strand in the presence of labeled nucleotides after capture of a specific DNA target. Using this method, we were able to sense the presence of labeled nucleotides in the femto-

(12) Knoll, W.; Zizlsperger, M.; Liebermann, T. S.; Badia, A.; Liley, M.; Piscevic, D.; Schmitt, F. J.; Spinke, J. *Colloids Surf., A* **2000**, *161*, 115−137.
(13) (a) Bos. L. W.; Lynch, D. W. *Phys. Rev. B* **1970**, *2*, 4567−4577. (b) Roy, D. *Opt. Commun.* **2001**, *200*, 119−130. (c) Roy, D. *Appl. Spectrosc.* **2001**, *55*, 1046−1052. (d) Chah, S.; Yi, J.; Pettit, C. M.; Roy, D.; Fendler, J. H. *Langmuir* **2002**, *18*, 314−318. (e) Ando, E.; Suzuki, S. *J. Non-Cryst. Solids* **1997**, *281*, 68−73.
(14) (a) Tasara, T.; Angerer, B.; Damond, M.; Winter, H.; Dörhöfer, S.; Hubscher, U.; Amacker, M. *Nucleic Acid Res.* **2003**, *31*, 2636−2646. (b) Zuh, Z.; Waggoner A. S. *Cytometry* **1997**, *28*, 206−211. (c) Yo, H.; Chao, J.; Patek, D.; Mujumdar, R.; Mujumdar, S.; Waggoner, A. S., *Nucleic Acid Res.* **1994**, *22*, 3226−3232.

molar region. However, an artificial DNA template was used that contained only a single guanine base to be paired with labeled Cy5-dCTP. For natural DNA, problems arise from strong intramolecular quenching of the dye with an increasing number of incorporated labels. In experiments utilizing a similar primer/template duplex that contained several guanine bases in the 35-mer templating region, we found that the fluorescence yield could not be substantially improved by incorporation of a larger number of dyes. In contrast, a high label density reduced the fluorescence yield. This problem can be circumvented by careful adjustment of the mole fraction of labeled nucleotides to the number of available labeling sites in the DNA substrates. For our system, we found an optimal fluorescence yield for the incorporation of a single dye molecule per DNA strand. Since best results were achieved for low label concentrations and natural DNA usually contains all four different types of bases, one would not profit from using different types of labeled nucleotides. dCTP was used in this study since a tendency has been revealed for the incorporation to decrease from pyrimidine to purine within the fluoro-dNTP derivative groups. If necessary, Cy5-labeled analogues of all four nucleotides are commercially available to be applied in the extension assay in case the captured DNA sequence lacks guanine bases. In principle, surface plasmons can be excited by using lasers with wavelengths shorter than 632.8 nm. However, shorter wavelengths cause a broadening of the SPR curve (and the corresponding SPFS curve) and a decrease of the enhancement of the evanescent field due to stronger absorption by the gold film. For excitation in the green wavelength range, one can nicely compensate for this effect by using a less-absorbing silver surface, which would be only sealed with a thin gold layer to increase its resistance in aqueous solution.

The setup is compatible with array experiments in different modes. If only one type of chromophor is used it is sufficient to exchange the detector photodiode and photomultiplier by CCD cameras to produce microscopic images. For experiments that require a wavelength-dependent readout scheme, a diode array might be used as a detection unit. With these tools in hand, one could imagine resolving DNA sequences by labeling each type of dNTP with a different chromophor. Very well suited for this purpose were quantum dots, which exhibit very broad absorption spectra (enabling the use of only one excitation wavelength) but very sharp emission peaks that can be controlled by fine-tuning of the particle size.

CONCLUSIONS

SPR-SPFS experiments enable the consecutive determination of the physicochemical and chemical properties of surface-confined molecules/films. Utilizing an enzymatic primer extension assay, the hybridization of immobilized catcher DNA strands with complementary target DNA was proven by means of the incorporation of Cy5-labeled dCTP. The incorporation of dye into the synthesized DNA strands was sensitively sensed by SPFS, whereas the corresponding mass increase was not detectible by SPR. Due to the reproducibility of the sensor surface and of the enzymatic reaction, the observed SPR curves show similar resonance angle shift as the complete DNA double strand is synthesized in the presence of different mole fractions of the fluorophore-labeled dCTP. In contrast, the corresponding SPFS curves show a strong, concentration-dependent fluorescence signal. The observed SPR-SPFS signal indicates that the employed DNA polymerase prefers the natural nonlabeled nucleotides over modified nucleotide derivatives. Knowledge of the evanescent field within the sensor architecture is an essential prerequisite for this kind of quantitative estimation. Therefore, we demonstrated how to correct for the sample-to-sample variation caused by small differences in the optical properties of the metal films used in different experiments.

ACKNOWLEDGMENT

S.E. gratefully acknowledges support from the Thailand Research Fund (TRF Contract RSA/07/2545) and the Alexander von Humboldt (AvH) Foundation.

SUPPORTING INFORMATION AVAILABLE

Comparisons between the experimentally observed SPR curves (at $\chi = 1.00$) and the fitted SPR curves based on Fresnel equation; the SPR curves of the biotinylated SAMs employed in the experiments; SPR-SPFS curves at various mole fractions χ of Cy5-dCTP in the mixed dNTPs solution; and comparisons between the experimentally observed SPR curves of the completed double-strand P45/T50 with Cy5-dCTP incorporation and the fitted SPR curves. These materials are available free of charge via the Internet at http://pubs.acs.org.

Received for review March 22, 2004. Accepted June 7, 2004.

AC0495586